PAPER Special Section on Analog Circuits and Related SoC Integration Technologies

A High-Linearity 264-MHz Source-Follower-Based Low-Pass Filter with High-Q Second-Order Cell for MB-OFDM UWB

Hong ZHANG[†], *Member*, Xue LI[†], Suming LAI[††], *Nonmembers*, *and* Pinyi REN[†a)], *Member*

SUMMARY Source-follower-based (SFB) continuous-time low-pass filters (LPF) have the advantages of low power and high linearity over other filter topologies. The second-order SFB filter cells, which are key building blocks for high-order SFB filters, are often realized by composite source follower with positive feedback. For a single branch 2nd-order SFB cell, the linearity drops severely at high frequencies in the pass band because its slew-rate is restricted by the Q factor and the pole frequency. The folded 2nd-order SFB cell provides higher linearity because it has two DC branches, and hence has another freedom to increase the slew rate. However, because of the positive feedback, the folded and unfolded 2nd-order SFB cells, especially those with high Q factors, tend to be unstable and act as relaxation oscillators under given circuit parameters. In order to obtain higher Q factor, a new topology for the 2nd-order SFB cell without positive feedback is proposed in this paper, which is unconditionally stable and can provide high linearity. Based on the folded 2nd-order SFB cell and the proposed high-Q SFB cell, a 264 MHz sixth-order LPF with 3 stages for ultra wideband (UWB) applications is designed in 0.18 μm CMOS technology. Simulation results show that the LPF achieves an IIP3 of above 12.5 dBm in the whole pass band. The LPF consumes only 4.1 mA from a 1.8 V power supply, and has a layout area of 200 μm × 150 μm.

key words: *source-follower-based (SFB), low-pass filter, linearity, Q factor, stability, MB-OFDM UWB*

1. Introduction

Multi-band orthogonal frequency division multiplex (MB-OFDM) ultra-wideband (UWB) systems have attracted great interest due to their potential for high-speed wireless communications. The baseband of MB-OFDM UWB systems adopt 128-point OFDM modulation to obtain 528-MHz bandwidth and achieve up to 480-Mbps data rate [1]. In a MB-OFDM UWB receiver, a high-performance low-pass filter (LPF) with 264-MHz bandwith is indispensable to block interferers and provide anti-alias filtering. The large bandwith and requirements of high linearity and low power make the design of LPFs for UWB very challenging.

Among several possible solutions for continuous-time LPFs [2], active−RC and MOSFET-C filters provide very high linearity, but they are preferable for narrow-band applications [3]–[5], because large gain-bandwith product requiremens would lead to unacceptable power consumption. $G_m - C$ filters have higher power efficiency and are widely used in broadband applications [6]–[8]. However, as open-loop operational transconductance amplifiers (OTAs) present limited linearity, various additional circuitry must be adopted to linearize the OTAs [9]–[11], which increases power consumption and design complexity.

An alternate to the existing topologies is to use source followers and capacitors to realize low-pass filtering. The first reported source-follower-based (SFB) LPF comprises of two 2nd-order SFB stages implemented by composite source followers with positive feedback, providing very good linearity and low power consumption [12]. The SFB LPF for MB-OFDM UWB system in [13] consists of 6 1st-order SFB stages in ladder structure, and shows a remarkable low power consumption of less than 1 mW. However, the 2nd-order SFB cells in [12]and the negative 1st-order SFB cells in [13], especially those with high Q-factors, tend to be unstable under certain circuit parameters. Moreover, the linearity of the 2nd-order SFB cell drops severely at high frequencies because its slew-rate is restricted by the Q-factor and the pole frequency of the filter. These issues impose a limit to the achievable Q-factor of the 2nd-order SFB cell with positive feedback.

In this paper, the stability and the linearity of the 2nd-order SFB cell with positive feedback are analyzed in detail. Analysis shows that the folded 2nd-order SFB cell, which is introduced in [12] for low voltage applications, can provide higher linearity at high frequency because it has two DC branches, and hence has another freedom to increase the slew rate. In order to obtain higher Q, a new topology for the 2nd-order SFB cell without positive feedback is proposed, which is unconditionally stable and can provide high Q. Based on the folded 2nd-order SFB cell and the proposed high-Q SFB cell, a 264 MHz sixth-order LPF with 3 stages designed in 0.18 μm CMOS technology is presented. Simulation results show that the LPF achieves an IIP3 of above 12.5 dBm in the whole pass band and consumes 4.1 mA from a 1.8 V power supply.

2. Analysis of the 2nd-Order SFB Cell

2.1 Transfer Function

A simple source follower with a load capacitor is inherently a 1st-order low-pass filter, as shown in Fig. 1(a). However, this simple filter provide only a real pole, hence can not constitute high-order SFB filters by cascading several stages. The second-order SFB cell in [12] adopts a single-branch composite source follower with positive feedback to synthe-

Manuscript received October 14, 2010.
Manuscript revised January 13, 2011.

[†]The authors are with the School of Electronic and Information Engineering, Xi'an Jiaotong University, Xi'an, China.
[††]The author is with the Department of Electrical & Computer Engineering, Texas A&M University, TX 77843 USA.
a) E-mail: pyren@mail.xjtu.edu.cn (corresponding author)

DOI: 10.1587/transele.E94.C.999

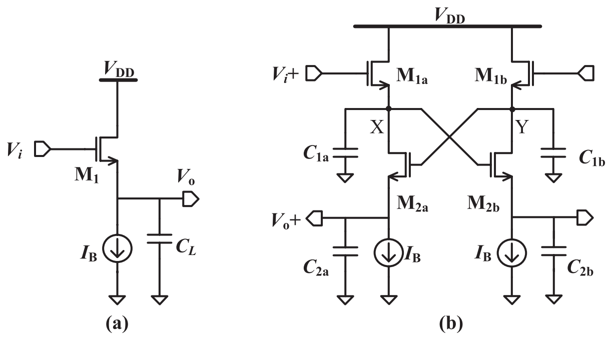

Fig. 1 (a) A 1st-order SFB LPF; (b) The 2nd-order SFB cell in [12].

size a pair of complex poles, as shown in Fig. 1(b). The cell can suppress even-order distortion extensively because of its fully differential structure. The output common-mode voltage is determined by V_{gs} of the transistors, hence no common-mode feedback circuit is needed.

The transfer function can be obtained from the half small-signal equivalent circuit. However, in [12], $M_{1a,b}$ and $M_{2a,b}$ are assumed to have same transconductance. This is not true even if the transistors have exactly the same sizes and all mismatches can be neglected, because the different source-to-substrate voltages of $M_{1a,b}$ and $M_{2a,b}$ will cause obvious difference between the transconductance of the transistors. Assuming the output conductance and parasitic capacitance of all transistors can be neglected, the transfer function of the 2nd-order SFB cell is re-derived as

$$H(s) = -\frac{1}{\frac{C_1 C_2}{g_{m1} g_{m2}} s^2 + [\frac{C_1}{g_{m1}} + (\frac{1}{g_{m2}} - \frac{1}{g_{m1}})C_2]s + 1} \tag{1}$$

where g_{m1} and g_{m2} are the transconductance of $M_{1a,b}$ and $M_{2a,b}$, C_1 and C_2 are the capacitance of $C_{1a,b}$ and $C_{2a,b}$, respectively. The transfer function has second-order low-pass characteristics with an unit DC gain. The result is the same as that in [12], if $g_{m1} = g_{m2}$. The pole frequency, ω_0, for Eq. (1) is calculated as

$$\omega_0 = \sqrt{\frac{g_{m1} g_{m2}}{C_1 C_2}} \tag{2}$$

which is also the same as that in [12] when $g_{m1} = g_{m2}$. Under the condition of $g_{m1} = g_{m2}$, $Q = \sqrt{C_2/C_1}$ [12], meaning that Q is only dependent on the ratio between the two capacitors. However, the difference between g_{m1} and g_{m2} can impose significant influence on the Q factor. In order to verify this, we define $n = C_2/C_1$, and $m = g_{m2}/g_{m1}$. The Q factor for Eq. (1) is derived as

$$Q = \frac{1}{\sqrt{m/n} + \sqrt{n/m} - \sqrt{m \cdot n}}. \tag{3}$$

When $m = 1$, Q equals to $\sqrt{n}$ exactly. Although the influence of m on Q can not be seen directly from Eq. (3), mathematical tools can be used to express the relation between them. Fig. 2 gives several curves of Q factor varying with capacitance ratio n under different transconductance ratio m. As stated in [12], Q increases with the square root of

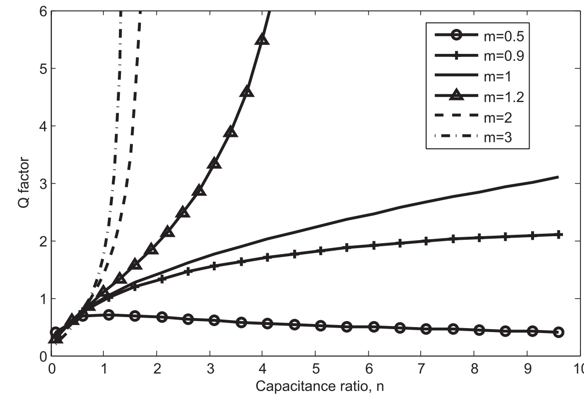

Fig. 2 Influence of transconductance ratio on the Q factor.

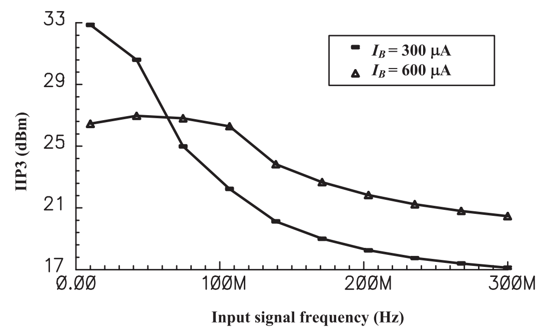

Fig. 3 IIP3 of the 1st-order SFB filter at different biasing current.

n, when $m = 1$. However, when $g_{m2} < g_{m1}$, i.e. $m < 1$, the increasing slope of the Q - n curve is reduced. If m is small enough, Q even decreases with n. On the other hand, when $g_{m2} > g_{m1}$, i.e. $m > 1$, Q is boosted extensively even with very small n. The Q will increase to infinity at certain values of capacitance ratio n, as shown in Fig. 2, which means that the circuit is unstable. This will be verified in Sect. 2.3.

2.2 Linearity Analysis

For the simple 1st-order SFB filter shown in Fig. 1(a), the linearity at low frequencies is higher with lower overdrive voltage of M_1, meaning that the linearity is improved by reducing bias current [12]. However, at high frequencies, the linearity is reduced at lower biasing current because of the limited slew rate. To verify this, a test circuit for the filter in Fig. 1(a) is designed, in which M_1 has a W/L of $10\mu/0.6\mu$, and C_L is 1.8 pF. The simulated pole frequencies are about 130 MHz at an I_B of 0.3 mA and increases to 150 MHz with I_B increasing to 0.6 mA. The IIP3 is simulated with two-tone sinusoid input signals that have a frequency deviation of 100 KHz. The simulated curves of IIP3 with sweeping input signal frequency are given in Fig. 3, which shows that the filter with larger biasing current (hence larger slew rate) has lower linearity at low frequencies, but provide higher IIP3 at high frequencies.

Above analysis for the 1st-order SFB filter can also be applied to the 2nd-order SFB cell. In the 2nd-order SFB cell

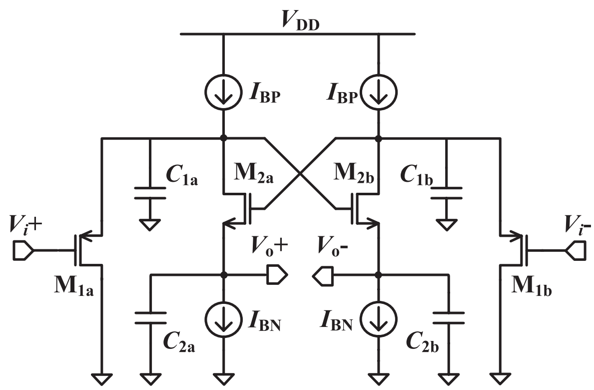

Fig. 4 Schematic of the folded 2nd-order SFB cell [12].

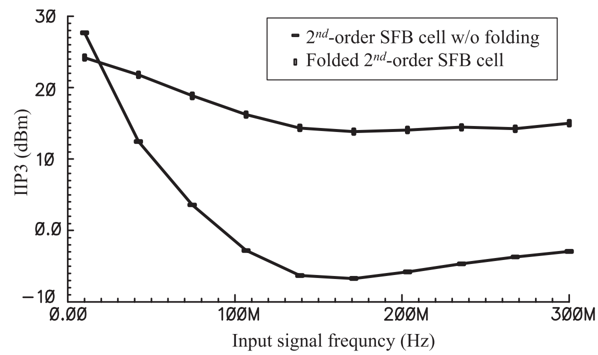

Fig. 5 Simulated IIP3 of the 2nd-order SFB cell with and without folding.

shown in Fig. 1(b), there are two pair of nodes that are influenced by charging of capacitors. For node X and Y, the response speed is enhanced by the positive feedback, hence the limited slew rate has little influence on them. However, the output nodes are similar with those in the 1st order cell, so the limited slew rate has significant impacts on the response speed of these nodes at high frequencies. In order to obtain higher linearity at high frequencies, the biasing current must be enlarged to some extent to increase the slew rate. However, enlarging I_B will increase both g_{m1} and g_{m2} because the cell has only single DC branch. From Eq. (2), the pole frequency ω_0 will increase with g_{m1} and g_{m2}. In order to keep ω_0 constant, C_2 and C_1 must be increased. This will in turn reduce the slew rate and the linearity. The transconductance can also be kept constant by decreasing the sizes of the transistors when I_B is increased. However, this will increase V_{gs} of the transistors, resulting in a reduced output swing of the cell.

Because the slew rate of the 2nd-order SFB cell is limited by its filtering characteristics, the linearity is dropped remarkably at high frequencies. The situations are more severe for those with higher Q factors, because C_2 is larger than C_1 in these cells, making the slew rate at the output nodes even lower.

The slew rate and hence the linearity at high frequencies can be improved with a folded 2nd-order SFB cell, which is introduced in [12] for low voltage applications, as shown in Fig. 4. The transfer function of the folded 2nd-order SFB cell is same as that of the cell in Fig. 1(a), because they have same small signal equivalent circuits. However, the folded 2nd-order SFB cell has two DC branches, hence has another freedom to increase the slew rate. From Fig. 4, the g_m of $M_{2a,b}$ is determined by I_{BN}, while the g_m of $M_{1a,b}$ is determined by $I_{BP} - I_{BN}$. In order to increase the slew rate at output nodes, I_{BN} can be increased independently. Although this will increase g_{m2} and hence alter the filtering characteristics, however, I_{BP} can be adjusted to change g_{m1} for compensation. According to Eqs. (2) and (3), adjusting of C_1 and C_2 are also needed to keep ω_0 and Q to the expected value. Although the tuning is a little complex, simulation can be used to refine the design.

Test circuites for the folded 2nd-order SFB cell and the cell shown in Fig. 1(b) are designed to compare the linearity. Both cells are designed with an ω_0 of about 200 MHz, and a Q of 1.5. The simulated IIP3 varying with input frequency for the two cells are given in Fig. 5, which show that the folded 2nd-order SFB cell provide superior linearity both at low and high frequencies. The unfolded cell consumes 0.6 mA, while the folded one consumes 0.72 mA from a 1.8 V power supply, which means that the great improvement in linearity is achieved only with a bit increase in power consumption. When Q increases to a larger value, even the folded 2nd-order SFB cell can not provide high IIP3 because C_2 becomes larger, resulting in decrease in slew rate at the output nodes. Furthermore, when Q is large enough, the circuit tends to oscillate, which will discussed in next section.

2.3 Stability Analysis

The positive feedback in the 2nd-order SFB cell, both for the folded and unfolded topology, can cause oscillation under certain circuit parameters, which is not discussed both in [12] and [13]. The structure of the 2nd-order SFB cell is inherently similar with a CMOS relaxation oscillator [14]. Considering the inner feedback loop, the 2nd-order SFB cell can be regarded as a two-stage inverting amplifier which are connected in ring topology. The rearranged small signal model is shown in Fig. 6, which is suitable for both the folded and unfolded 2nd-order SFB cell. In Fig. 6, $1/g_{m1}$ denotes the small-signal output resistance of $M_{1a,b}$ in both Fig. 4 and Fig. 1(b), while r_{ob} is the output resistance of the current source I_B, which is large and can be neglected for simplicity.

The open-loop gain of the whole circuit is the square of the transfer function of each stage. After simple calculation, the open-loop gain of the circuit in Fig. 6 is obtained as

$$H_O(s) = \left[\frac{g_{m2}C_2 s}{(g_{m2} + C_2 s)(g_{m1} + C_1 s)}\right]^2 \tag{4}$$

which shows that a single stage has a zero at DC, and two poles at $-\frac{g_{m2}}{C_2}$ and $-\frac{g_{m1}}{C_1}$, respectively. According to Barkhausen criterion, the circuit will oscillate at frequency ω_0, if $|H_O(j\omega_0)| = 1$, and $\angle H_O(j\omega_0) = 360°$. Combining

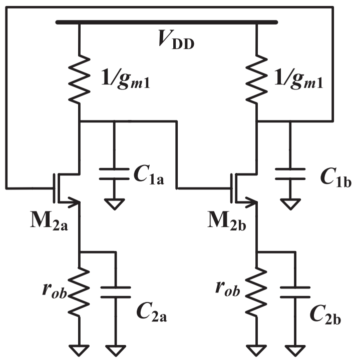

Fig. 6 Small signal model of the 2nd-order SFB cell's inner loop.

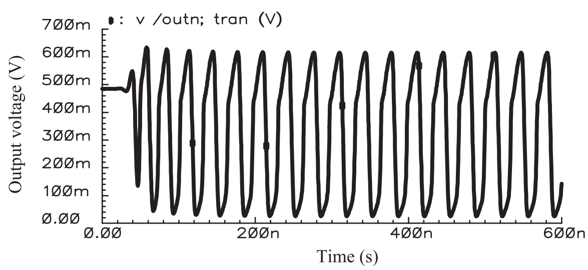

Fig. 7 Simulated oscillation wave of the 2nd-order SFB cell with $m = 3$, and $n = 2$.

these two conditions with Eq. (4), the oscillation will occur if the following equation is satisfied:

$$\frac{g_{m2}}{g_{m1}} = \frac{C_2}{C_2 - C_1}. \tag{5}$$

Using the definition of $m = g_{m2}/g_{m1}$ and $n = C_2/C_1$, the oscillation condition is simplified to

$$m > \frac{n}{n-1} \tag{6}$$

Eq. (6) is only valid for either $m > 1$, or $n > 1$, because the magnitude of the open-loop gain is always less than 1 and the circuit is unconditional stable when either $m < 1$, or $n < 1$. Applying Eq. (6) into Eq. (3), Q is calculated to be infinity for all possible n, which validates the oscillation condition. The oscillation is also verified by transient simulation of the test circuit in Sect. 2.2 with $m = 3$, and $n = 2$. Simulated results show that the circuit oscillates without any input signal, with the oscillation wave at one of the output node shown in Fig. 7.

As can be seen from Eq. (6), in order to guarantee stable operation of the 2nd-order SFB cell, m must be smaller than $n/(n-1)$, which results in significant decrease in the achievable Q. Figure 8 gives several curves of Q varying with n, under different scaling coefficients of m. Although higher maximum Q can be obtained with larger scaling coefficient, however, in order to ensure stability, the scaling coefficient should be less than 0.7, leading to a maximum achievable Q of less than 5.

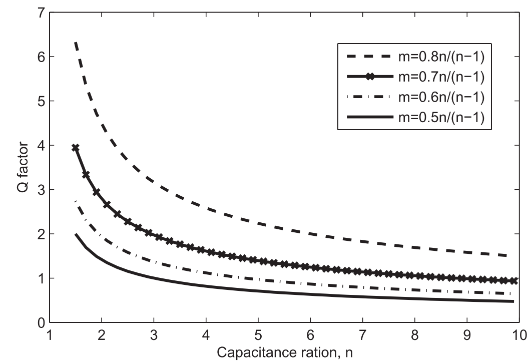

Fig. 8 Curves of Q factor varying with n under different scaling coefficients of m.

3. The Proposed High-Q 2nd-Order SFB Cell

From the analysis in Sect. 2, the folded 2nd-order SFB cell is suitable for implementing filter sections with low and medium Q factor, as its Q factor is limited by slew rate and stability. However, high-Q 2nd-Order cells are necessary to implement high-order filters with good performance. For example, in a 6th order Chebyshev filter, a high-Q 2nd-order section with large peaking is needed to compensate the loss of other two sections with low and medium Q factors at high frequencies, and make the filter show sharp roll-off and small ripples in its pass band.

In order to realize a high-Q 2nd-Order SFB cell with high linearity, a new topology based on the method of improving the linearity of source followers in [15] is proposed in this paper, as shown in Fig. 9. The cell includes a main composite source follower that is composed of $M_{1a,b}$, $M_{4a,b}$ and $M_{7a,b}$, and a inverting amplifier comprising $M_{2a,b}$ and $M_{3a,b}$. The inverting amplifier provides negative feedback to improve voltage transferring accuracy of the main source follower in large voltage swing and hence improve the linearity at low frequencies. For example, if V_i+ increases, V_o+ will increase by the same amount in ideal situation. However, I_{BP} will decrease slightly because of the channel length modulation effect of M_{7a}. In order to accommodate the slight decrease in I_{BP}, V_{sg} of M_{1a} must be decrease, resulting in that V_o+ has smaller amount of increase than V_i+, which will cause nonlinearity at low frequencies. Furthermore, because I_{BP} decreases, V_{sd} of M_{1a} will also decreases by a small amount because of the channel length modulation effect, which means that the drain voltage of M_{1a} will increase slightly.

In the proposed circuit, the inverting amplifier is used to detect the voltage variation in the drain node of $M_{1a,b}$, and adjust the current flowing in $M_{2a,b}$ and $M_{3a,b}$. Because of the feed back provided by the inverting amplifier, I_{BP} can be kept constant even the input voltage has a large swing. In Fig. 9, by using the source follower composed of $M_{5a,b}$ and $M_{6a,b}$, current reusing for $M_{3a,b}$ is realized to provide additional gain in the feedback loop, and hence improve the linearity further.

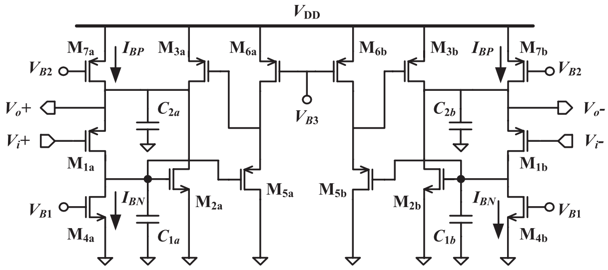

Fig. 9 Schematic of the proposed high-Q 2nd-Order SFB cell.

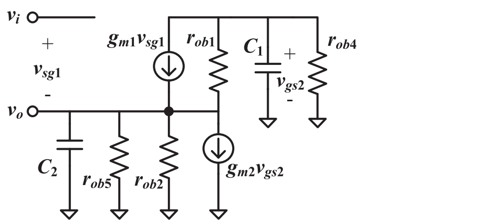

Fig. 10 Half small signal of the proposed high-Q 2nd-Order SFB cell.

Because this cell is used to implement high-Q sections, C_2 is usually larger than C_1, which means that the linearity at high frequencies is mainly determined by the slew rate at the output nodes. However, as shown in Fig. 9, the response speed of the output nodes is enhanced significantly by the inverting amplifier through injecting current to these nodes, hence the linearity will not limited by the slew rate.

The transfer function of the proposed cell can be obtained with the half small signal equivalent circuit, as shown in Fig. 10. In Fig. 10, g_{m1} is the tansconductance of $M_{1a,b}$, and g_{m2} denotes the transconductance sum of $M_{2a,b}$ and $M_{3a,b}$. Resistors r_{ob1}, r_{ob4}, and r_{ob5} are the output resistance of $M_{1a,b}$, $M_{4a,b}$, and $M_{5a,b}$, respectively, while r_{ob2} is the parallel of the output resistance of $M_{2a,b}$ and $M_{3a,b}$. After neglecting parasitic capacitance and output resistance, the transfer function for the proposed cell is derived as

$$H(s) = \frac{\frac{C_1}{g_{m2}} \cdot s + 1}{\frac{C_1 C_2}{g_{m1} g_{m2}} s^2 + \frac{C_1}{g_{m2}} \cdot s + 1} \tag{7}$$

which has 2nd-order low-pass characteristics. The pole frequency ω_0 and Q factor are calculated to be

$$\begin{cases} \omega_0 = \sqrt{\frac{g_{m1} g_{m2}}{C_1 C_2}} \\ Q = \sqrt{\frac{g_{m2} C_2}{g_{m1} C_1}} \end{cases} \tag{8}$$

As can be seen from Eq. (8), the expression for ω_0 is same as that of the 2nd-order cell with positive feedback, while the expression of Q is more concise. Because no positive feedback exists in the proposed cell, very high Q can be obtained with large ratio of g_{m2}/g_{m1} and C_2/C_1. The disadvantage of the proposed cell is the zero at $\omega_z = -g_{m2}/C_1$, as shown by Eq. (7). However with large Q factors, ω_z is much larger than ω_0, and has negligible influence on the roll off performance. To verify this, two cells that have Q factors of 6.5 and 1.2 respectively are simulated for comparison. Both cells are designed with same ω_0 of about 250 MHz. Simulated curves of transfer function magnitude are given in Fig. 11, which shows that the cell with high Q factor provide sharper roll-off performance because of the larger distance between the zero and the poles. Therefore, the proposed 2nd-Order SFB cell is only suitable for implementing high-Q filter sections.

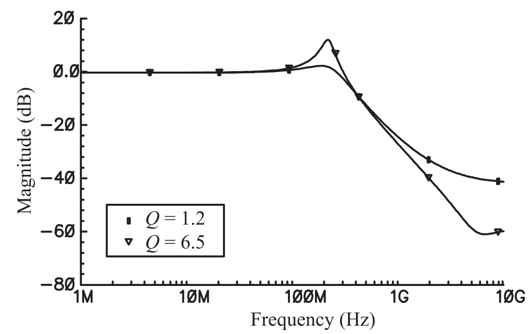

Fig. 11 Simulated output amplitude for the proposed cells with high and low Q factors.

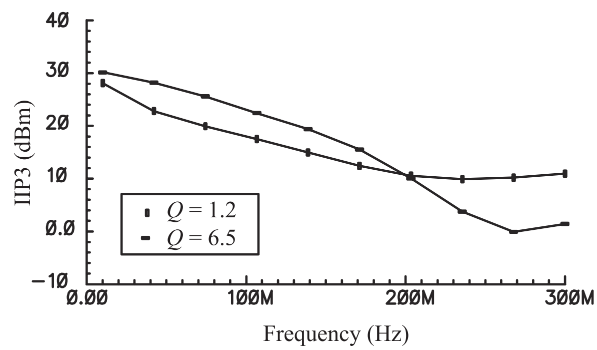

Fig. 12 Simulated IIP3 of the proposed cells with high and low Q.

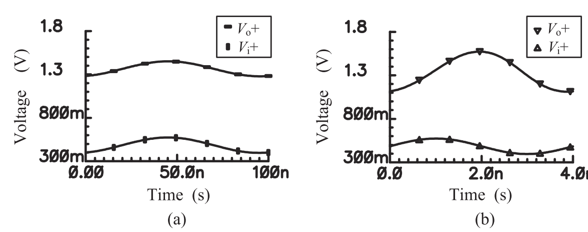

Fig. 13 Input and output voltage of the proposed cell with Q = 6.5 at (a) 10 MHz; (b) 250 MHz.

The linearity for the above two cells are also simulated, with results shown in Fig. 12. As can be seen, IIP3 of the cell with $Q = 6.5$ drops remarkably at high frequencies. This is mainly due to the large phase shifting between the input and output voltage and the peaking in the magnitude at high frequencies. Fig. 13 shows the waveforms of the input and output voltage for the cell with $Q = 6.5$ at 10 MHz and 250 MHz. When the input signal is at 10 MHz, the phase shift between the input and output voltage is close to zero and the voltage gain is nearly 1, hence the output voltage follows the input with very high accuracy. However, when the input frequency increases to 250 MHz, the phase shift is nearly $\pi/2$ and the output voltage is amplified because of the peaking at this frequency, as shown in Fig. 13. The large phase shift together with the peaking at high frequencies causes significant distortion in g_{m1}, resulting in remarkable reduction of IIP3. The deterioration of linearity for the proposed high-Q cell is caused inherently by the voltage transfer characteristics, and hence can not be solved by enlarging bias current. However, as will discussed in the next section, the linearity reduction of this cell can be compensated by placing it at the last stage, ensuring high IIP3 for the whole filter at all frequencies.

4. Design of the Sixth-Order MB-OFDM UWB Filter

MB-OFDM UWB systems provide high data rate up to 480 Mbps by adopting 128-point OFDM modulation in baseband to obain 528-MHz bandwidth. To block the strong interferences and provide anti-alias filtering for ADCs, a 264 MHz bandwidth LPF with high linearity is indispensable in the analog baseband. Furthermore, in order to suppress the signal in adjacent UWB channels, the attenuation at 528 MHz is required to be at least 30 dB.

In order to achieve the requirements of sharp roll-off, a six-order Chebyshev (type-I) prototype function with 1 dB passband ripple is adopted for the MB-OFDM UWB filter in this paper. The filter is divided into three 2nd-order SFB stages, with specifications of Q and f_0 given in Table 1. Based on the analysis in Sects. 2 and 3, the folded 2nd-order SFB cell in Fig. 4 is adopted to implement stage I and II, because they have low and medium Q factors. Stage III with Q of 6.5 is realized by the proposed high-Q 2nd-Order SFB cell shown in Fig. 9.

The arrangement of the position for the three stages has significant influence on the overall linearity performance of the filter, because the high-Q stage has limited IIP3 at high frequencies. The relation of the overall IIP3 between the IIP3 of each stage can be expressed as

$$\frac{1}{IIP3_{total}^2} = \frac{1}{IIP3_I^2} + \frac{A_{v,I}^2}{IIP3_{II}^2} + \frac{A_{v,I}^2 A_{v,II}^2}{IIP3_{III}^2} \tag{9}$$

where $IIP3_I$, $IIP3_{II}$, $IIP3_{III}$ are the IIP3 in voltage for stage I, II, and III, while $A_{v,I}$, and $A_{v,II}$ are voltage gain of stage I and II, respectively. From Eq. (9), stage I should be the first stage as it provide the highest IIP3, while stage III should be the last stage because it has the poorest IIP3 at high frequencies. This is contrary to stage arrangement in normal cascading systems, such as amplifiers with gain larger than one. As shown in Table 1, because stage I and II have lower pole frequencies, their voltage gain will attenuated to very low value at the frequencies where peaking occurs in stage III, hence the IIP3 reduction at high frequencies in stage III is compensated extensively by the first two stages. As a result, very good linearity is obtained in the whole passband for the overall filter.

Table 1 Pole frequencies and Q factors of the 2nd-order stages.

	Stage I	Stage II	Stage III
f_0 (MHz)	103	202.8	267
Q	0.7	1.8	6.5

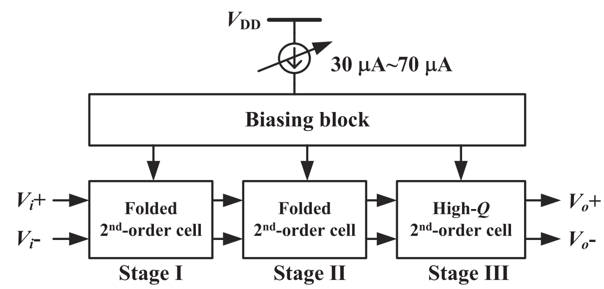

Fig. 14 Block diagram of the proposed sixth-order MB-OFDM UWB filter.

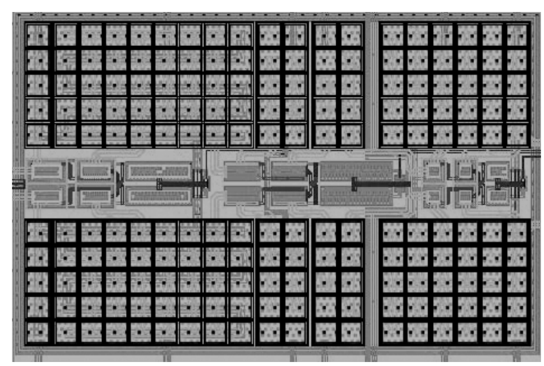

Fig. 15 Layout of the proposed sixth-order MB-OFDM UWB filter.

The block diagram of the proposed six-order MB-OFDM UWB filter is given in Fig. 14. The three stages are connected directly by DC coupling. In order to cope with the bandwith variations caused by temperature and process, a biasing circuit with a variable reference current source is adopted to adjust the transconductance of the transistors in the filter stages. The tuning can be realized either in analog or digital domain.

The proposed filter is designed in the TSMC 0.18 μm CMOS technology, and has a layout area of 200 μm × 150 μm, as shown in Fig. 15. The capacitors in the filter are realized by metal-insulator-metal (MIM) capacitors.

5. Simulation Results

The simulation is carried out in Cadence Analog Design Environment after layout parasitic extraction. The simulated curves of the transfer function for the filter at different biasing current are shown in Fig. 16. As can be seen, the filter shows nominal transfer function with −3-dB bandwith at 264 MHz when the input reference current is 50 μA. The attenuation at 528 MHz is 41 dB, which is much larger than the requirement. The tuning range of −3-dB bandwith is

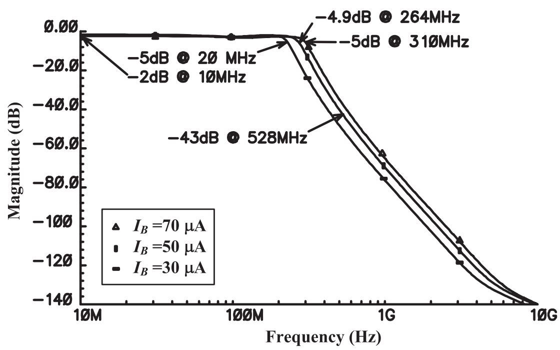

Fig. 16 Magnitude of transfer function at different bias current.

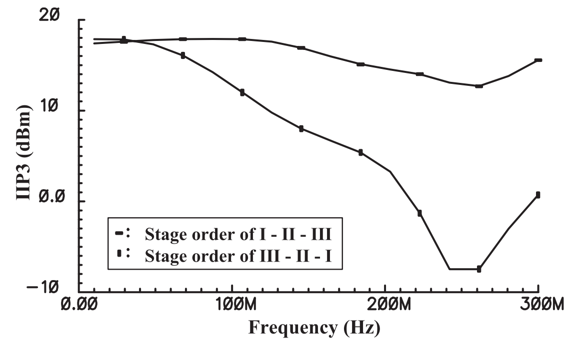

Fig. 18 IIP3 varying with input frequency.

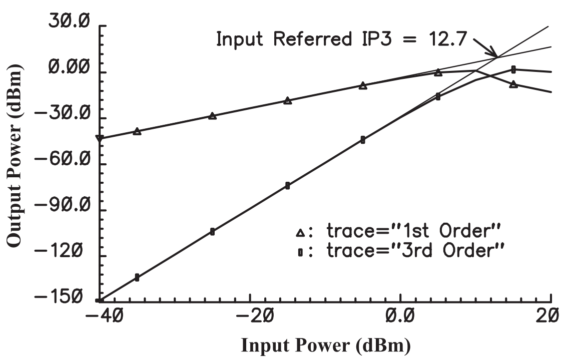

Fig. 17 IIP3 with two-tone input at 250 MHz and 250.1 MHz.

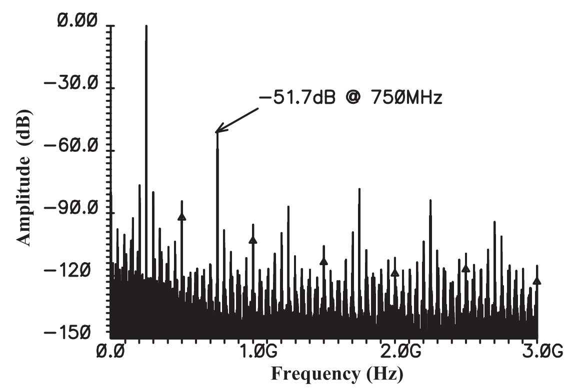

Fig. 19 Third-order distortion with input V_{pp} of 500-mV at 250-MHz.

from 201 MHz to 310 MHz when the input reference current varies from 30 μA to 70 μA, which can cover the bandwith variations caused by process and temperature. The non-ideal voltage transfer characteristics of the source followers causes 2-dB loss at low frequencies.

The IIP3 is 12.7 dBm with two-tone input signals at 250 MHz and 250.1 MHz, as shown in Fig. 17. The simulated curves of IIP3 varying with input frequencies are obtained by sweeping the two-tone frequency, and are given in Fig. 18. In order to show the influence of stage arrangement on the overall linearity, the proposed filter with stage order of I–II–III and another filter with stage order of III–II–I are simulated for comparison. Notice that, the output DC level of stage III is too high to provide proper operating point for stage II in the modified filter with reverse order. Therefore, ideal DC biasing and AC coupling are adopted in the filter sections for the modified filter to ensure that it has the same DC operating point and almost the same AC transfer function as the proposed filter, hence making the linearity comparison effective. As can be seen in Fig. 18, the IIP3 of the proposed filter is very high at low frequencies, and reduced to a minimum value of 12.5 dBm at 264 MHz. After that frequency, IIP3 begins to increase because of the fast attenuation of amplitude in the transfer function. On the other hand, the IIP3 of the modified filter with reverse order drops severely at high frequencies in the passband, which validates the analysis of stage arrangement in Sect. 4.

The proposed filter shows very low third-order harmonic distortion even at high input frequencies. As seen from Fig. 19, the third-order harmonic distortion is −51.7 dB with input V_{pp} of 500 mV at 250 MHz.

The integrated input-referred noise in the pass-band of the proposed filter is 594 μV, corresponding to an input referred noise density (IRND) of 37 nV/$\sqrt{\text{Hz}}$. In a full-band MB-OFDM UWB receiver, the input bandwith is 7.5 GHz (3.1 GHz to 10.6 GHz), leading to an input noise power of approximately −75 dBm. If the proposed filter is used in an UWB receiver with a RF frond-end gain of 35 dB, its noise power referred to the input of the receiver is about −86.4 dBm, which is much smaller than the input noise power of the receiver.

The maximum group delay of 4.7 ns occurs at the frequency where stage III have the maximum peaking, as shown in Fig. 20. The proposed filter draws 4.1 mA from a 1.8 V power supply.

Performance comparisons with other broadband filter are given in Table 2. As can be seen, the proposed filter shows higher linearity with low power consumption. However the IRND of the proposed filter is larger than those in [7] and [8], which is mainly due to the small capacitance values used in the filter sections. According to the derivations in [12], the noise power in SFB filters is inversely proportional to capacitance values. Therefore, the noise power can be reduced by using larger capacitance values. However, this will increase the chip area, and the current consumption must be enlarged to maintain other performances. Fortunately, as stated above, the noise performance requirements

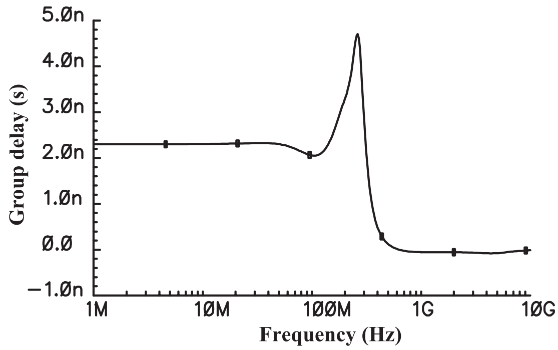

Fig. 20 Group delay of the proposed filter.

Table 2 Performance comparisons.

	[7]	[8]	[9]	[13]	This work
Filter type	$G_m - C$	$G_m - C$	$G_m - C$	SFB	SFB
Filter order	5	5	7	6	6
−3 dB BW (MHz)	240	275	200	280	264
IIP3	−48 dBV	−12 dBV	–	11 dBm*	12.5 dBm
HD3 (dB)	–	–	−44	–	−51.7
Power diss. (mW)	24	36	60	0.12	7.4
Technology (nm)	130	65	350	–	180
IRND (nV/ $\sqrt{\text{Hz}}$)	7.7	7.8	65	–	37
Area (mm^2)	0.34	0.21	1.8	0.01	0.03

*The input frequency for measuring IIP3 is not given.

of the filter in UWB applications is relatively low because of the large input noise power of the receiver. Therefore, the noise performance of the proposed filter is acceptable in MB-OFDM UWB applications.

6. Conclusions

In this paper, the transfer function, linearity and stability of the unfolded and folded 2nd-order SFB LPF cells are analyzed in detail. A new topology of 2nd-order SFB cell without positive feedback capable of providing high Q factor with stable operation is proposed. Based on the folded 2nd-order SFB cell and the proposed high-Q 2nd-order SFB cell, a 264-MHz sixth-order LPF designed in 0.18 μm CMOS technology for MB-OFDM UWB systems is presented. Simulation results show that the filter achieves an minimum IIP3 of 12.5 dBm in the whole passband. The filter consumes 4.1 mA from a 1.8 V power supply and has a layout area of 200 μm × 150 μm.

Acknowledgments

This work was supported by the Research Fund for the Doctoral Program of Higher Education of China, under the grant of 20090201120025.

References

[1] A. Batra, J. balakrishnan, G.R. Aiello, J.R. Foerster, and A. Dabak, "Design of a multiband OFDM system for realistic UWB channel environments," IEEE Trans. Microw. Theory Tech., vol.52, no.9, pp.2123–2138, Sept. 2004.

[2] Y. Tsividis, "Continuous-time filters in telecommunication chips," IEEE Commun. Mag., vol.163, no.4, pp.132–137, 2001.

[3] S. D'Amico, V. Giannini, and A. Baschirotto, "A 1.2 V-21 dBm OIP3 4th-order active-gm-RC reconfigurable (UMTS/WLAN) filter with on-chip tuning designed with an automatic tool," European Solid-State Circuits Conf., pp.315–318, 2005.

[4] A. Yoshizawa and Y.P. Tsividis, "Anti-blocker design techniques for MOSFET-C filters for direct conversion receivers," IEEE J. Solid-State Circuits, vol.37, no.3, pp.357–364, March 2002.

[5] H. Shin and Y. Kim, "A CMOS active-RC low-pass filter with simultaneously tunable high- and low-cutoff frequencies for IEEE 802.22 applications," IEEE Trans. Circutis Syst. II, Express Briefs, vol.57, no.2, pp.85–89, Feb. 2010.

[6] A. Lewinski and J. Silva-Martinez, "A 30-MHz fifth-order elliptic low-pass CMOS filter with 65-dB spurious-free fynamic range," IEEE Trans. Circutis Syst. I, Regular Papers, vol.54, no.3, pp.469–480, March 2007.

[7] V. Saari, M. Kaltiokallio, S. Lindfors, J. Ryynanen, and K. Halonen, "A 1.2 V 240 MHz CMOS continuous-time low-pass filter for a UWB radio receiver," Int. Solid-State Circuits Conf., pp.122–124, 2007.

[8] V. Saari, M. Kaltiokallio, S. Lindfors, J. Ryynaen, and K. Halonen, "A 240-MHz low-pass filter with variable gain in 65-nm CMOS for a UWB radio receiver," IEEE Trans. Circutis Syst. I, Regular Papers, vol.56, no.7, pp.1488–1499, July 2009.

[9] J. Silva-Martinez, J. Adut, J.M. Rocha-Perez, M. Robinson, and S. Rokhsaz, "A 60-mW 200-MHz continuous-time seventh-order linear phase filter with on-chip automatic tuning system," IEEE J. Solid-State Circuits, vol.38, no.2, pp.216–225, Feb. 2003.

[10] A. Lewinski and J. Silva-Martinez, "A linearity enhancement technique for high frequency applications with IM3 below 65 dB," IEEE Trans. Circutis Syst. II, Express Briefs, vol.51, no.10, pp.542–548, Oct. 2004.

[11] M. Mobarak, M. Onabajo, J. Silva-Martinez, and E. Sanchez-Sinencio, "Attenuation-predistortion linearization of CMOS OTAs with digital correction of process variations in OTA-C filter applications," IEEE J. Solid-State Circuits, vol.45, no.2, pp.351–367, Feb. 2010.

[12] S. D'Amico, M. Conta, and A. Baschirotto, "A 4.1-mW 10-MHz fourth-order source-follower-based continuous-time filter with 79-dB DR," IEEE J. Solid-State Circuits, vol.41, no.12, pp.2713–2719, Dec. 2006.

[13] S. D'Amico, M.D. Matteis, and A. Baschirotto, "A 6th-order 100 μA 280 MHz source-follower-fased single-loop continuous-time filter," Int. Solid-State Circuits Conf., pp.72–73, 2008.

[14] B. Razavi, "A study of phase noise in CMOS oscillators," IEEE J. Solid-State Circuits, vol.31, no.3, pp.331–343, March 2010.

[15] S. Lai, H. Zhang, and G. Chen, "An improved source follower with wide swing and low output impedance," IEEE Asia-Pacific Conf. on Circuits and Systems, pp.814–817, 2008.

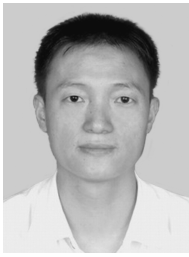

Hong Zhang received the B.S. degree in electronic engineering from Xi'an University of Technology in 2000 and the M.S. and Ph.D. degrees from Xi'an Jiaotong University, Xi'an, China, in 2004 and 2008, respectively. Since 2008, He has been with the Department of Microelectronics, where he is an associate professor. His interests include CMOS Mixed-signal and RF IC design.

Xue Li received the B.S. degrees in electronic science and technology from Xi'an Jiaotong University, Xi'an, China, in 2010. She is currently working toward the M.S. degree at the same University. His research interests include CMOS mixed-signal IC design.

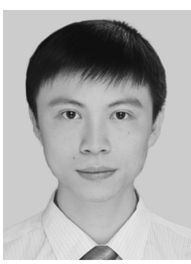

Suming Lai received the B.S. and M.S. degrees in electronic science and technology from Xi'an Jiaotong University, Xi'an, China, in 2006 and 2009, respectively. He is currently working toward the Ph.D. degree at the Department of Electrical & Computer Engineering, Texas A&M University, TX 77843 USA. His research interests include CMOS mixed-signal and RF IC design.

Pinyi Ren received the Ph.D. degree from Xi'an Jiaotong University, Xi'an, China, in 2001. He is a professor in the Department of Information and Telecommunication Engineering, Xi'an Jiaotong University, China. His current research interests include wireless communication, signal detection and cognitive radio systems and networking.